Available online at www.sciencedirect.com
SCIENCE DIRECT®
Journal of Catalysis 220 (2003) 74–83
JOURNAL OF CATALYSIS
www.elsevier.com/locate/jcat

The relevance of Ru nanoparticles morphology and oxidation state to the partial oxidation of methane

Ioan Balint,[a,*] Akane Miyazaki,[b] and Ken-ichi Aika [b]

[a] *Institute of Physical Chemistry, Romanian Academy, Spl. Independentei 202, 77208 Bucharest, Romania*
[b] *Department of Environmental Chemistry and Engineering, Interdisciplinary Graduate School of Science and Technology, Tokyo Institute of Technology, 4259 Nagatsuta, Midori-ku, 226-8502 Yokohama, Japan*

Received 10 February 2003; revised 12 May 2003; accepted 19 June 2003

Abstract

The partial oxidation of methane over well-defined Ru nanoparticles supported on alumina was investigated in the 350–650 °C temperature range. A 12% Ru/Al_2O_3 catalyst was prepared by deposition of relatively monodispersed colloidal Ru nanoparticles of about 5.8 nm on alumina. The evolution of the chemical state and the morphology of Ru nanoparticles under the reaction conditions were followed by various techniques (TEM, H_2 chemisorption, XRD, TPR, and TPO). The experimental results suggest that the mechanism of partial oxidation of methane over the catalyst is related to the morphology (size) and chemical state of the supported Ru nanoparticles, as well as on the nature of the oxidizing agent (i.e., O_2 and NO). The formation of an abundant RuO_2 phase in the reaction mixture ($CH_4/O_2 = 1.8$), which is favored in the low-temperature region, was found to be responsible for the conversion of methane to total oxidation products. The $RuO_2 \Leftrightarrow$ Ru equilibrium is shifted to the formation of Ru metal for reaction temperatures higher than 450 °C. At that moment, the reaction became ignited because of a change in the reaction mechanism. Above the ignition temperature, the reaction rate increased considerably, and CO and H_2 were simultaneously produced. In the high-temperature region the mass transport phenomena affects the reaction rate as well as the product distribution. A relationship between the reaction temperature and the ratio between RuO_2 and total amount of Ru was quantitatively determined. At low temperatures, the alumina-supported Ru nanoparticles (initial size ≈5.8 nm) show significantly higher catalytic activity and selectivity to CO and H_2, than the conventionally prepared catalysts. For example, the yields to CO and H_2 at 650 °C were 72.1 and 67.6%, respectively. The idea that the high catalytic performance of Ru nanoparticles can be ascribed to the better preservation of the metallic character under the reaction conditions as compared to the well-dispersed Ru particles is advanced. A brief reaction mechanism is proposed in light of the experimental results.

Keywords: Ru catalyst; Methane partial oxidation; Ru nanoparticles; Ru oxidation state; Ru morphology; Mass-transport effects

1. Introduction

The partial oxidation of methane (POM) with air or oxygen is of great practical and academic interest [1,2]. Supported Ru catalysts proved to be among the best catalytic systems for POM reactions. Although supported Ru catalysts have been intensively investigated, there are still several aspects that need to be clarified in the future. The morphological evolution of the supported Ru nanoparticles under the reaction conditions has been relatively little investigated. A recently published work shows clearly that the morphological effects are quite important when CH_4 undergoes partial oxidation with NO [3]. Along the morphological evolution in time, the oxidation state of the supported Ru particles is likely to change as a function of reaction conditions (temperature, nature of oxidant, and mixture composition). Ru metal has a relatively high chemical reactivity, being relatively easily reduced or oxidized as a function of experimental conditions. There is a lack of information regarding the chemical state (oxidation state) of the supported metal during the POM reaction. Some studies suggested the ruthenium enrichment of the catalytically active surface during POM reactions [4] but a clear, quantitative estimation as a function of reaction conditions has not been made to this point. Another unsolved problem is related to the primary reaction

* Corresponding author.
E-mail addresses: balint@chemenv.titech.ac.jp, ibalint@chimfiz.icf.ro (I. Balint), akanem@chemenv.titech.ac.jp (A. Miyazaki), kenaika@chemenv.titech.ac.jp (K.-i. Aika).

0021-9517/$ – see front matter
doi:10.1016/S0021-9517(03)00279-3

products, as well as the relationship between product distribution and chemical state of the supported Ru nanoparticles. There is contradicting information regarding the origin of the reaction products over supported Ru catalysts. Some studies claim that CO and H_2 are the primary reaction products [5] whereas other authors suggest that the combustion of methane is followed by CH_4/CO_2 and CH_4/H_2O reforming reactions to generate CO and H_2 [6,7]. To this point, the mass transfer effects were little considered when reaction kinetics was proposed. Since the hydrocarbon oxidation reactions are exothermic processes, it is likely that the reaction becomes ignited when the temperature reaches a critical point. Above the ignition temperature, the mass transfer processes may disguise the surface kinetics of the reaction. It is clear that there is a need to analyze more carefully the mass transfer effect on the distribution of the POM reaction products (CO and H_2).

To conduct a meaningful investigation on the morphology vs catalytic reactivity relationship, a starting catalyst with well-defined metal particles should be prepared. The conventional preparation methods have several disadvantages: the size of the resulting metal particles cannot be well controlled, and the interaction with the support (support effect) is little understood. Particularly, for the conventionally prepared catalyst, strong support effects have been found in POM over ruthenium catalysts [8,9]. A practical way to prepare well-defined metal particles is the colloid route. The major advantages of this method are that it provides relatively monodispersed metal particles, and the size of these particles can be tuned to some extent by changing the preparation variables (i.e., precursor concentration, pH, temperature of reduction) [10].

The general aim of the present research is to investigate the relationship between the catalytic reactivity and the chemical state (oxidation state) as well as the morphology (size) of the alumina-supported Ru nanoparticle. Additionally, a closer look will be taken to assess the mass transfer effects on catalytic activity and selectivity.

2. Experimental

A 12% Ru/Al_2O_3 catalyst was prepared by reduction of a $RuCl_3$ precursor with ethylene glycol in the presence of γ-Al_2O_3 (Aerosil, 95.7 $m^2\,g^{-1}$). The preparation procedure was described in detail a previous work [10]. Briefly, alumina was added under stirring to the ethylene glycol solution containing the dissolved the $RuCl_3{\cdot}3H_2O$ (Wako Chemicals, purity > 99%) to form a suspension. Then, the temperature was raised slowly to 180 °C to allow the reduction of $RuCl_3$ by the ethylene glycol on the surface of alumina. After the ruthenium reduction was completed, the ethylene glycol was removed by diluting the suspension with 0.3 M $NaNO_3$. The solid phase was collected by filtration, washed several times with distilled water, and dried at room temperature in vacuum. The sodium content of the catalyst was below the detection limit (< 1 ppm) of ICP (inductively coupled plasma spectroscopy; Seiko SPS 4000). Prior to ICP analysis the catalyst was dissolved in an autoclave at 150 °C, 12 h, using a mixture of HF–NNO_3–$HClO_4$ acids.

The amount of supported Ru was estimated by ICP from the metal concentrations in the suspension before reduction, and in filtrate after reduction.

The catalyst was characterized in different stages by TEM (transmission electron microscopy; Philips CM 20) and by XRD (X-ray diffraction; Rigaku Multiflex apparatus provided with peak assignment software).

Temperature-programmed reduction (TPR) and temperature-programmed oxidation (TPO) experiments were carried out in a flow system, with 0.1 g of catalyst, using a Chembet 3000-Quantachrome Instruments type apparatus equipped with thermal conductivity detectors (TCD). Additionally, the species evolved during TPR and TPO experiments were analyzed with a quadrupole mass spectrometer (Anelva M-Q200TS). The gas mixtures used in TPR and TPO measurements were 3% H_2 in Ar and 3% O_2 in He, respectively. The typical heating rate was 10 °C min^{-1} and the total flow rate of the oxidizing or reducing gaseous mixtures was 70 ml min^{-1}. A silicagel water trap was interposed between the analyzed sample and the TCD detector in order to ensure a good stability and sensitivity of the detection system.

Activity tests for POM reactions were performed at atmospheric pressure with 0.05 g of catalyst (0.3- to 1-mm fraction) loaded in a U-shapped quartz microreactor (i.d. = 5 mm). The small diameter (i.d. = 2 mm) of the reactor outlet was designed to minimize the homogeneous secondary reactions taking place after the reactant stream passed through the catalytic bed. Taking into account the reduced size of the catalytic reactor (length and diameter) as well as the high GHSV operating values we assume that the homogeneous conversion of methane was minimized. The blank tests with the reactor containing only quartz wool, using O_2/CH_4 as reactant mixture, revealed that the homogeneous conversion of CH_4 starts from $T > 850$ °C (the highest temperature in our study was 650 °C). Prior to the activity tests the catalyst was conditioned at 500 °C in O_2 (30 min) and H_2 (30 min) to remove the small amount of organic phase (ethylene glycol) remaining from the preparation stage. The reactor was heated with a furnace connected to a temperature controller (Shimaden, Model SR 25). The reactant mixtures were prepared using electronic flow controllers (Kofloc, Model 3660). The typical total flow rate of the CH_4/O_2 and CH_4/NO mixtures was 50 ml min^{-1} STP (standard temperature and pressure). The corresponding GHSV (gas hourly space velocity) was 60,000 h^{-1}. The specific reactant compositions were 10.6% CH_4 and 5.9% O_2 in N_2 and 10.5% CH_4 and 13% NO in Ar.

The gaseous mixtures to and from the reactor were analyzed with a GL Science chromatograph (Model 320) equipped with TCD detectors. The H_2, O_2, CH_4, NO, and CO were separated and analyzed by using a molecular sieve

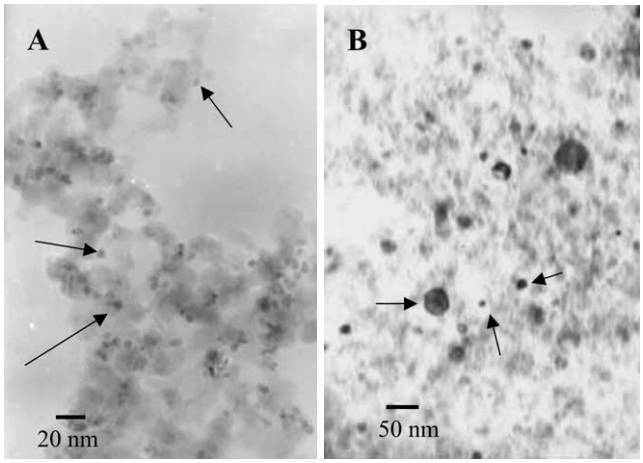

Fig. 1. TEM photo of the alumina-supported Ru nanoparticles. (A) Fresh (as prepared) and (B) used catalyst (650 °C, 1 h).

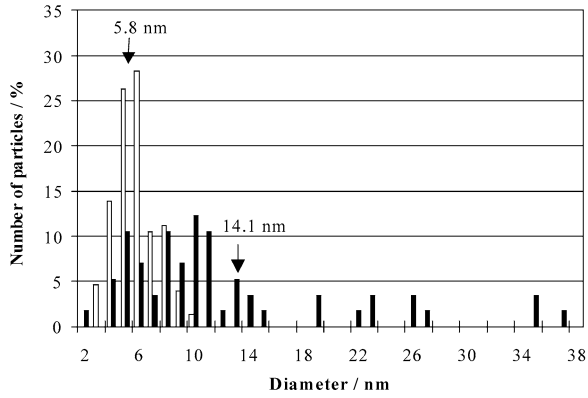

Fig. 2. Evolution of the size distribution under POM reaction conditions for alumina-supported Ru nanoparticles. □, as-prepared colloidal Ru nanoparticles (fresh 12% Ru/Al_2O_3 catalyst); ■, catalyst working for 1 h at 650 °C in reaction mixture (10.6% CH_4, 5.9% O_2, and balance Ar).

5 Å column whereas CO_2 was determined with a Porapaq-Q column.

The BET surface area of the Ru/Al_2O_3 catalyst was determined by N_2 physisorption at −196 °C. The surface area of Ru metal, dispersion (expressed as percentage), and particles size (assuming a spherical geometry and $H_{ads}/Ru = 1$ stoichiometry) were measured by H_2 chemisorption at 45 °C. The physisorption as well as chemisorption measurements were carried out with the same apparatus used for TPO and TPR investigations.

3. Results

The preparation variables have a great impact on the final morphology of the alumina-supported Ru nanoparticles. The reduction temperature and concentration of $RuCl_3$ in ethylene glycol optimal to obtaining spherical shaped and relatively uniform Ru nanoparticles were found to be 180 °C and 10^{-3} M, respectively. One important advantage of the polyol method is that metal loading onto support can be increased up to 12% or even higher without affecting the particle size or dispersion [10]. The typical morphology of the colloidal Ru nanoparticles supported on alumina (fresh catalyst) is presented in Fig. 1A. In addition, Fig. 1B shows the TEM image of the Ru nanoparticles for the working catalyst exposed to the reaction mixture at 650 °C for 1 h. It can be observed that under reaction conditions, the Ru particle size increased. It appears that under reaction conditions the Ru metal particles spread on the support and then emerge in larger particles. The size distribution and the average size (d_{TEM}) of the Ru nanoparticles for the fresh and used catalyst were statistically determined from TEM micrographs by counting more than 200 particles (Fig. 2). The initial size distribution of the Ru nanoparticles was relatively narrow, ranging between 2 and 10 nm. The maximum of the Gaussian-type distribution is located at 5.8 nm (see also Table 1). The preconditioning of the catalyst (at 500 °C for 30 min in O_2 and then for other 30 min in H_2) led to an increase in the average size of the Ru nanoparticles to 7.4 nm (Table 1). As can be seen from Table 1, the average size of the Ru nanoparticle for the spent catalyst (1 h in reaction mixture at 650 °C) ranges between 12 and 15 nm, depending slightly on the determination method. The size distribution of the Ru particles in the used catalyst became significantly broader, ranging between 2 and 38 nm. The average size of this catalyst determined from TEM micrographs (d_{TEM}) was 14.1 nm (Fig. 1B and Table 1). The average size values of the metal particles, estimated by H_2 chemisorption (d_{chem}) and from the line broadening of Ru (101) XRD reflection at $2\theta \approx 44°$, were 12 and 15 nm, respectively. The further increase of the Ru particles in time, under reaction conditions, was slower. After a long time on stream (i.e., 48 h at 650 °C) in a reducing atmosphere ($CH_4/O_2 = 1.8$), the size of the Ru particles size was stabilized at ≈ 19 nm (no further sintering was observed). On the other hand, Ru coarsening was accelerated in an O_2-rich atmosphere ($CH_4/O_2 \approx 0.5$). In the oxidizing mixture, the average size of Ru particles increased

Table 1
Average size of Ru nanoparticles of 12% Ru/Al_2O_3 catalysts, as determined from TEM micrographs, by H_2 chemisorption, and by XRD

Catalyst stages	S_{BET}[a] ($m^2\,g^{-1}$)	Dispersion[b] (%)	S_{Ru}[c] ($m^2\,g^{-1}$)	d_{Ru} (nm)		
				H_2 chemisorption[d]	XRD[e]	TEM
Fresh[f]	72	–	–	–	–	5.8
Pretreated[g]	–	18.0	7.9	7.4	–	–
Used[h]	68	11.2	4.9	12.0	15.0	14.1

[a] Physical surface area determined by N_2 adsorption at −196 °C.
[b] Ru dispersion determined by H_2 chemisorption at 45 °C.
[c] Ru metal surface determined by H_2 chemisorption.
[d] Ru average particle size determined by H_2 chemisorption.
[e] Ru particle size determined from the line broadening of Ru(101) XRD reflection at $2\theta \approx 44°$.
[f] As-prepared colloidal Ru nanoparticles supported on Al_2O_3.
[g] Catalyst pretreated successively with O_2 and H_2 at 500 °C for 30 min.
[h] Catalyst used for 1 h in CH_4 (10.6%)–O_2 (5.9%) reaction mixture at 650 °C.

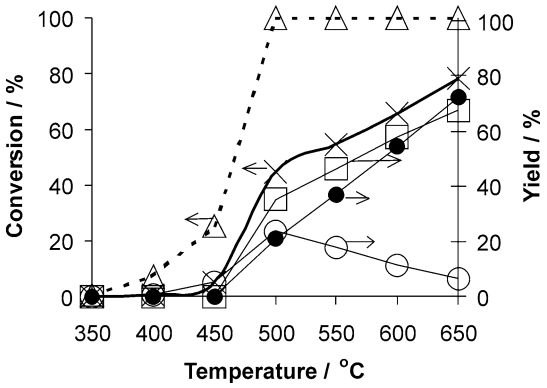

Fig. 3. The conversion of CH_4 (×) and O_2 (△) as well as the reaction yields to H_2 (□), CO (●), and CO_2 (○) as a function of temperature for 12% Ru Al_2O_3 catalyst. Reaction mixture was 10.6% CH_4, 5.9% O_2, and balance N_2.

progressively with reaction temperature up to 29.1 nm at 650 °C. It is obvious that the Ru sintering is a complex phenomenon, being strongly related to the reaction conditions (temperature, composition of the reactant mixture, and time on stream). Therefore, to establish a clear relationship between the morphology as well as the chemical state of Ru particles and catalytic reactivity, the experimental conditions should be carefully selected and clearly specified. The following discussion will be focused on the morphological and chemical state of Ru nanoparticles under CH_4-rich conditions ($CH_4/O_2 = 1.8$).

Fig. 3 illustrates the dependence of catalytic activity on the reaction temperature for the 12% Ru/Al_2O_3 catalyst. The S-type dependence of methane conversion on the reaction temperature is typical for exothermic reactions [11]. Three temperature-related regions can be distinguished from the evolution of methane conversion with temperature. At low temperatures (350–450 °C), the reaction rate increased exponentially with temperature (region I). CH_4 was converted slowly and selectively to the total oxidation products, CO_2 and H_2O. The highest CH_4 and O_2 conversions observed in region I at 450 °C, were 5.2 and 25.2%, respectively. The oxygen consumption at 450 °C is slightly higher than the stoichiometric one; this can be attributed to the massive oxidation of the Ru metal. This aspect will be analyzed in more detail under Discussion. The subsequent increase in reaction temperature led to a sudden increase in reaction rate (region II). Under our experimental conditions, the light-off temperature was observed in the 450–500 °C temperature domain (see Fig. 3). After the O_2/CH_4 reaction was ignited, the conversion of O_2 reached 100% and the generation of large amounts of CO and H_2 started. For example, the reaction yields to CO and H_2 at 500 °C were 20.8 and 35.4%, respectively. The reaction yield to CO_2 jumped from 5.2% at 450 °C to 23.7% at 500 °C. Above the ignition temperature ($T > 450$ °C, region III) the increase in methane conversion with temperature became slower. The amounts of CO and H_2 showed an increasing trend with temperature, whereas the formation of CO_2 had an opposite trend. The highest yields

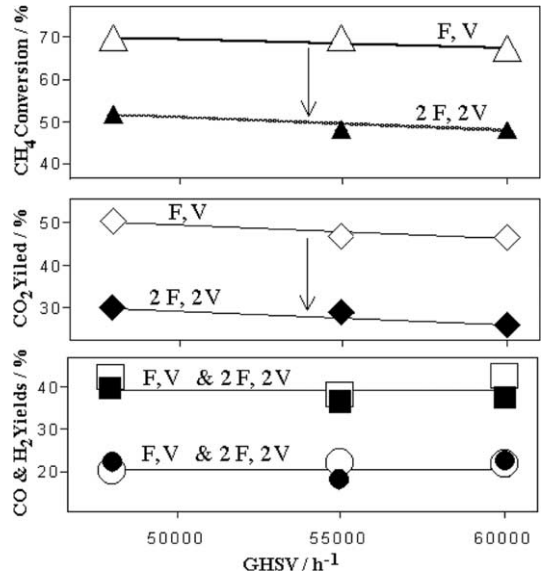

Fig. 4. The influences of catalyst GHSV (gas space hourly space velocity) on CH_4 conversion (△, ▲) and POM reaction yields to CO (○, ●), CO_2 (◆, ◇), and H_2 (□, ■) at 500 °C. F and V represent the flow rate and catalyst volume, respectively.

to CO and H_2, observed at 650 °C, were 72.1 and 67.6 %, respectively. At the same temperature the CO_2 yield dropped to 6.3% (see Fig. 3).

In the upper temperature region ($T \geqslant 500$ °C) the reaction rate was affected by the flow rate of the reactant mixture (F) and the volume of catalyst (V). Fig. 4 shows the influence of GHSV ($F \times V^{-1}$) on CH_4 conversion and yields to reaction products (CO, H_2, and CO_2) at 500 °C. The CH_4 conversion and reaction yield to CO_2 at constant GHSV values decreased significantly when the flow rate and the catalyst volume (weight) were concomitantly doubled. The drop in CH_4 conversion and yield to CO_2 were ≈ 20%. The CH_4 conversion and yield to CO_2 exhibited a slight decreasing trend with raising the flow rate of the reactant mixture. On the other hand, the reaction yields to CO and H_2 were not affected by the catalyst amount or by the reactant flow rate. The dependence of CH_4 conversion on catalyst amount and gas flow rate suggests that the processes in region III are influenced by mass transport phenomena. This aspect will be analyzed in more detail later.

First, the effect of reaction mixture composition {$[O_2]/[CH_4]$} on the $[CO_2]/[CO]$ ratio as well as on the ignition temperature in the region III (500–650 °C) was examined. This investigation was conducted to gather information regarding the primary reaction products over Ru/Al_2O_3 catalysts. Fig. 5 shows that the ignition temperature is not affected by the composition of the reaction mixture. Other C_1 combustion studies, conducted on supported Pt, found also that the light-off temperature is not strongly related on the mixture composition [12]. Methane-rich reaction mixtures ($[O_2]/[CH_4] < 1$) give generally larger amounts of CO than CO_2. For $[O_2]/[CH_4] > 1.1$, the $[CO_2]/[CO]$ ratio sharply increases with oxygen concentration (Fig. 5). The increase

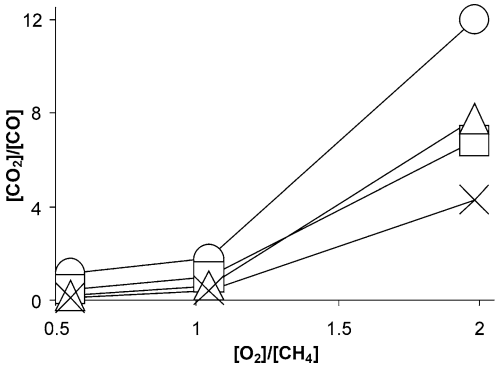

Fig. 5. The relationship between the reactant composition (expressed as the molar ratio between O_2 and CH_4) and $[CO_2]/[CO]$ ratio determined for the 12% Ru/Al_2O_3 catalyst in the 500–650 °C temperature range. (○) 500; (△) 550; (□) 600; and (×) 650 °C.

of CO_2/CO ratio with increasing oxygen concentration for $T \geqslant 500$ °C indicates that the primary reaction products (CO and H_2) are oxidized by the excess oxygen to CO_2 and H_2O, after formation. The increase of the reaction temperature led to a decrease in CO_2 production, even in oxygen-rich mixtures ($O_2/CH_4 \approx 2$), because the O_2 is preferentially consumed in partial oxidation of methane. It is well known that the POM reaction is thermodynamically favored at higher temperatures [13,14].

The next step of the study consisted in the identification of the reasons responsible for the sudden change in the CH_4/O_2 reaction mechanism that occurs in the 450–500 °C temperature interval. It is essential to understand the reasons why the reaction ignition is accompanied by the simultaneous generation of CO and H_2. The influence of oxidant agent on Ru chemical state was also investigated by using NO instead of O_2. In order to get information on the working state of Ru under the reaction conditions, the catalyst was rapidly cooled (≈ 600 °C/min) to room temperature under high-purity inert gas (Ar). Then, the state of the 12% Ru/Al_2O_3 catalyst at various temperatures was investigated by XRD, TPR, and TEM.

The comparative XRD spectra of the 12% Ru/Al_2O_3 catalyst after working for 1 h in a O_2–CH_4 reaction mixture (10.6% CH_4, 5.9% O_2, and balance N_2) at 450 (spectrum c), 550 (spectrum d), and 650 °C (spectrum e) are presented in Fig. 6A. The same figure contains the XRD spectra of the alumina support (spectrum a) and alumina-supported colloidal Ru nanoparticles (fresh catalyst) (spectrum b). Fig. 6B shows the XRD spectra of the catalyst used 1 h in a NO–CH_4 reaction mixture (10.5% CH_4, 13% NO, and balance Ar) at 450 (spectrum f), 550 (spectrum g), and 650 °C (spectrum h). The following observations can be made from analysis of the XRD spectra. The absence of any detectable Ru crystallite peaks for the alumina-supported colloidal Ru nanoparticles (Fig. 6A, spectrum b) indicates that the average crystallite size in the fresh catalyst is below the detection level by XRD ($d \leqslant 6$ nm). This result is expected since the average diameter determined by TEM was 5.8 nm. The catalyst used for the O_2–CH_4 reaction in the 450–650 °C temperature range shows the well-defined XRD reflections of Ru metal as well as relatively diffuse XRD peaks characteristic for RuO_2 (Fig. 6A, spectra c–e). The relative heights of the Ru and RuO_2 peaks are related to the reaction temperature. The highest intensity of the $RuO_2(110)$ XRD reflection at $2\theta \approx 28°$ was observed for the catalyst that has worked in reaction mixtures at 450 °C (Fig. 6A, spectrum c). Interestingly, the intensity of the $RuO_2(110)$ peak decreased for higher reaction temperatures, i.e., 550 °C (Fig. 6A, spectrum d) and 650 °C (Fig. 6A, spectrum e). On the other hand, sharper and better resolved XRD peaks, characteristic for Ru metal, were evident in the high temperature region (550 and 650 °C). The XRD spectra obtained after the catalyst was exposed to a NO–CH_4 mixture are even more suggestive. The supported ruthenium was extensively oxidized at 450 and 550 °C under reaction conditions to RuO_2 and the characteristic XRD reflections of Ru metal cannot be observed (Fig. 6B, spectra f, g). On the other hand, the catalyst used at 650 °C (Fig. 6B, spectrum h) gives only the XRD peaks of Ru metal. The XRD results suggest a progressive reduction of the RuO_2 phase to Ru metal in both reaction mix-

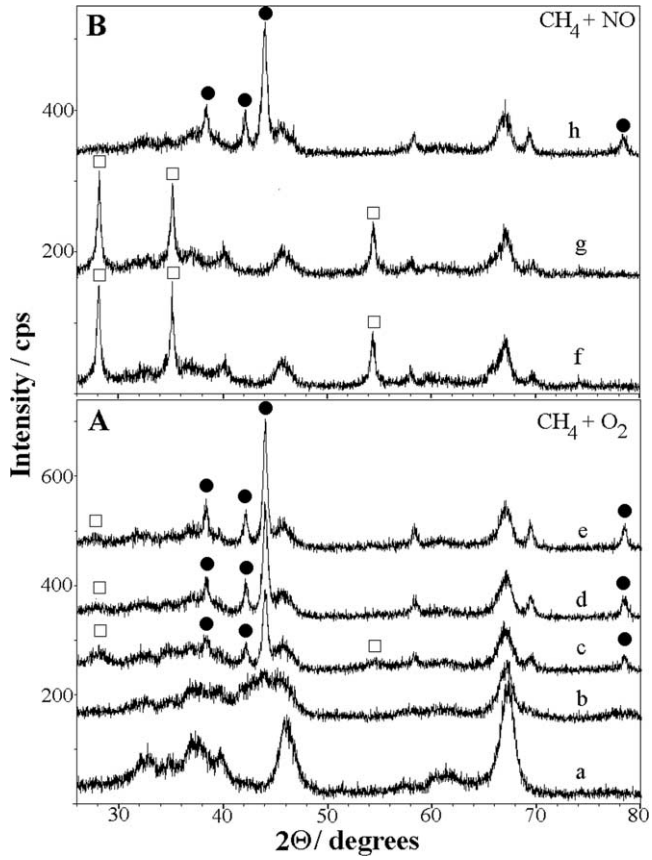

Fig. 6. The XRD spectra of the 12% Ru/Al_2O_3 catalyst in different stages. (A) Al_2O_3 support (a), colloidal Ru supported on Al_2O_3 (b), and catalyst working for 1 h in CH_4 (10.6%)–O_2 (5.9%) reaction mixture at 450 (c), 550 (d), and 650 °C (e). (B) catalyst exposed 1 h to CH_4 (10.5%)–NO (13%) reaction mixture at 450 (f), 550 (g), and 650 °C (h). (●) Ru, (□) RuO_2.

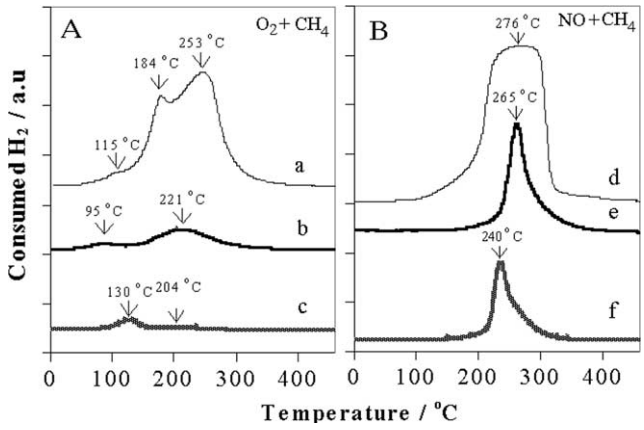

Fig. 7. The TPR patterns of the 12% Ru/Al_2O_3 catalyst working 1 h in (A), CH_4 (10.6%)–O_2 (5.9%) and (B), CH_4 (10.5%)–NO (13%) reaction mixtures at 450 °C (patterns a and d), 550 °C (patterns b and e), and 650 °C (patterns c and f). The composition of the mixture used in TPR experiments was 3% H_2 in Ar.

tures (O_2–CH_4 and NO–CH_4) as the reaction temperature increases. The XRD investigation reveals also that ruthenium is more severly oxidized by a reaction mixture close to a stoichiometric one ($C/O \approx 0.85$) when NO is used as oxidizing agent. A quantitative estimation of the RuO_2/Ru_{Total} ratio by using XRD technique is difficult. A limitation of the XRD method is the lack of sensitivity in detecting low amounts of a given phase (in our case RuO_2) in a heterogeneous catalyst [15]. Therefore, a phase playing an important catalytic role might be greatly underestimated or even overlooked.

The TPR technique was chosen to investigate the relationship between the chemical state of the supported ruthenium and the reaction temperature. The comparative TPR spectra of the 12% Ru/Al_2O_3 catalyst used for O_2–CH_4 reactions at 450 (pattern a), 550 (pattern b), and 650 °C (pattern c) are presented in Fig. 7A. The TPR patterns obtained from the catalyst exposed to NO–CH_4 mixtures at 450 (pattern d), 550 (pattern e), and 650 °C (pattern f) are shown in Fig. 7B. We assume that ruthenium state under reaction conditions was not significantly altered during the rapid cooling of the catalyst (0.1 g) to room temperature under pure Ar. The H_2 consumption in TPR runs was ascribed to the reduction of RuO_2 since no other stable ruthenium oxides are known to exist in the solid state [16]. The release of species other than water (i.e., CH_4), resulting from the hydrogenation of the eventually existing carbonaceous deposits, could not be observed by a mass spectrometer. The results presented in Fig. 7 clearly show that, for a given composition of the reaction mixture, the amounts of RuO_2 and Ru metal in the active catalyst are related to the reaction temperature and to the nature of the oxidizing agent. Large amounts of RuO_2 are formed under reaction conditions at 450 °C (Fig. 7, spectra a and d). The reduction of the supported RuO_2 particles is a size-dependent process. Two TPR peaks have been observed for the catalyst used for O_2–CH_4 reactions at 450 °C (Fig. 7A, pattern a). The high-temperature peak (for our catalyst, at 253 °C) can be attributed to the reduction of large RuO_2 particles, whereas the low-temperature peak (in our case, at 184 °C) can be assigned to the reduction of the well-dispersed (small) RuO_2 particles [17]. The catalytic tests with O_2–CH_4 show that at 450 °C CH_4 is slowly transformed (conversion was only $\approx 7\%$) to total oxidation products (CO_2 and H_2O). The increase in reaction temperature led to a significant decrease in the amount of RuO_2 contained by the active catalyst. The catalyst used at 550 and 650 °C for O_2–CH_4 reactions gave TPR peaks at 221 °C (Fig. 7A, pattern b) and 204 °C (Fig. 7A, pattern c), respectively. Those TPR peaks are significantly smaller than those of the catalyst used at 450 °C (Fig. 7A, pattern a). The small TPR peaks observed in the 95–130 °C temperature interval can be attributed either to the H_2 chemisorption on Ru metal or to the reduction of tiny RuO_2 particles.

At each temperature investigated, the amount of RuO_2 formed under reaction conditions was larger for the catalyst working in NO–CH_4 mixtures (Fig. 7B). The broad TPR peak that can be observed at a given reaction temperature can be attributed to the extensive oxidation of Ru by NO–CH_4 mixtures. As in the case of the O_2–CH_4 system, the amount of RuO_2 decreased with increasing reaction temperature along with the shift of maximum position to lower temperatures (Fig. 7B, spectra d–f).

The fact that the $RuO_2 \Leftrightarrow$ Ru equilibrium shifts to the right-hand side as the reaction temperature increases suggests that a change should also take place in the reaction mechanism. The catalytic tests show clearly that the sudden increase in reaction rate, observed in the 450–500 °C temperature range, is accompanied by the generation of large amounts of CO and H_2 (see Fig. 3). A strong support effect was observed in the case of the conventionally prepared catalysts having well-dispersed (small) Ru particles. It seems that, in contrast to TiO_2, Al_2O_3 has a tendency to stabilize ruthenium in the ionic state (reduction temperature > 700 °C) [8]. Our TPR results presented in Fig. 7 show that the large ruthenium nanoparticles supported on alumina can be easily reduced at significantly lower temperatures (up to 400 °C). It is clear that in the case of the catalyst prepared via colloid deposition, the support interaction with the catalytically active phase is minimized [10]. Thus, the catalytic activity can be ascribed mainly to the intrinsic properties of Ru nanoparticles.

Since the mechanism of POM reaction seems to be related to the $RuO_2 \Leftrightarrow$ Ru equilibrium, the oxidation of the alumina-supported Ru nanoparticles was investigated by TPO (Fig. 8). The oxidation rate of the Ru nanoparticles reaches a maximum at 594 °C. The TPO as well as TPR results suggest that the ruthenium oxidation-reduction kinetics depends on the composition of the reaction mixture, temperature, and particles size.

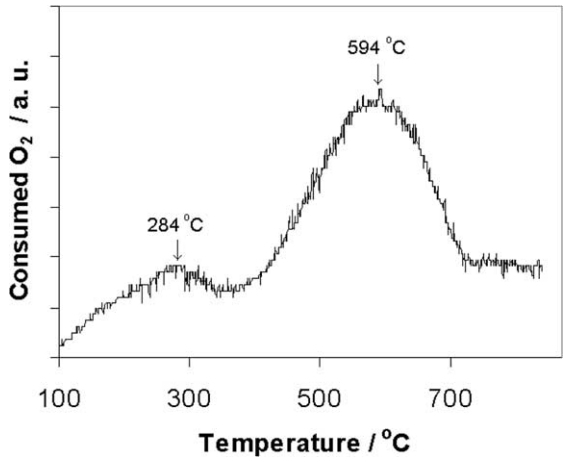

Fig. 8. The TPO pattern obtained for 12% Ru/Al_2O_3 (0.1 g) catalysts conditioned at 500 °C in O_2 (30 min) and then in H_2 (30 min). The composition of the mixture used in TPO experiments was 3% O_2 in He.

4. Discussion

4.1. Kinetic and transport effects

There are several published works investigating the kinetics of partial oxidation of methane over conventionally prepared supported Ru catalysts. It is somehow surprising that the diffusion effects on the reaction are little considered when a reaction mechanism is proposed. The S-shape dependence of methane conversion on temperature, presented in Fig. 3, is typical for exothermic processes (i.e., combustion reactions) [11]. Three regions can be distinguished. At low temperatures ($T \leqslant 450\,^{\circ}\mathrm{C}$), when the reaction rate is small in comparison with the diffusion rate, the overall rate of the process is determined by the surface kinetics (kinetic region). The reaction rate increases exponentially with temperature, in accordance with Arrhenius expression, and does not depend on the flow velocity of the gas. The further increase in temperature lead to a point where the reaction rate becomes equal to the diffusion rate. When the heat released by surface reaction exceeds a critical value, the reaction becomes self-accelerated (ignition). The newly developed stationary state is strongly affected by mass-transport limitations [18,19]. The sharp increase of the reaction rate (inflammation) was observed under our experimental condition in a narrow temperature range (between 450 and 500 °C). In some cases the formation of hot spots in the catalytic bed under the condition of partial oxidation of methane was observed [20]. Although it cannot be ruled out, the formation of hot spots could not be observed experimentally in our conditions. As in the case of methane combustion, it is likely that after ignition a sufficient number of free surface sites (i.e., Ru metal) would be available for adsorption of methane and oxygen. In this case the global process is limited by diffusion of reactants toward the catalyst and products away from the catalyst [21,22]. After reaction inflammation (region III), the reaction rate increase with temperature is moderate, because it is limited by diffusion processes.

In the kinetic region ($T \leqslant 450\,^{\circ}\mathrm{C}$), methane is converted slowly and selectively to CO_2 and H_2O over the 12% Ru/Al_2O_3 catalyst (see Fig. 3). The temperature dependence of methane conversion during partial oxidation and combustion is relatively similar, but the distribution of reaction products is different. With few exceptions, methane is selectively converted over supported Pt or Pd catalysts to total oxidation products (CO_2 and H_2O) in a broad temperature region. Only at high temperatures ($T \approx 1100\,^{\circ}\mathrm{C}$) and very short residence time (10^{-4} s) the formation of partial oxidation products was observed [23]. The supported Ru catalyst behaves completely different in the kinetic region and in the diffusion domain. The formation of CO and H_2 can be observed only above ignition temperature (Fig. 3).

The mass transfer effects were investigated by observing the influence of the catalyst volume (V) and methane flow rate (F) on the reaction rate and yield of products. The results presented in Fig. 4 show a drastic decrease in methane conversion at a twofold increase in the catalyst volume and gas flow rate. The drop in methane conversion was accompanied by a similar decrease in the reaction yield to CO_2, while the yields to CO and H_2 remained unaffected. The observed changes can be explained by a simple model which accounts for the effect of mass transfer on conversion and selectivity. The conversion can be defined as the ratio between CH_4 reacted ($[CH_4]_{\mathrm{reacted}}$, mol s^{-1}) and the CH_4 inlet (F, mol s^{-1}). The relationship between CH_4 conversion (X, %), F and V (mL) can be expressed as:

$$X = \left\{[\mathrm{CH_4}]_{\mathrm{reacted}}/F\right\} \times 100 = \left[(R_{\mathrm{CH_4}} \times V)/F\right] \times 100 = R \times \mathrm{GHSV}^{-1} \times 100,$$

$R_{\mathrm{CH_4}}$ is the CH_4 reaction rate (mol mL^{-1} s^{-1}). In the absence of mass transport effects, the methane conversion should be independent of V and F (or on GHSV). In fact, we observed that methane conversion decreased with $\approx 20\%$ when the catalyst volume (or weight) and flow rate were doubled (for $2V$ and $2F$) (see Fig. 4). If R is constant at a given temperature, it comes out that the decrease in CH_4 conversion can be viewed as an apparent decrease in the catalyst volume (V). From Fig. 4 it can be observed that F has relatively low impact on methane conversion (X). The decrease in CH_4 conversion, taking place when the catalyst volume and flow rate were simultaneously increased, can be explained by the decrease in the catalytically active surface area that becomes available to the reactants. In other words, the reactants diffusion to the catalytically active sites is hindered when the catalyst amount is increased. The diffusion inside catalyst pores seems to be the more likely reason for the observed mass transfer limitation. The apparent decrease in catalyst volume can be viewed as a decrease of the effective contact time ($V \times F^{-1}$ or GHSV^{-1}) between the reactants and the catalyst surface. Shorter contact time means that the secondary oxidation reactions, such as $CO \rightarrow CO_2$ and $H_2 \rightarrow H_2O$, are partially prevented. This hypothesis explains well the decrease in CO_2 yield, as well as the increase

in selectivity to H_2 and CO, when the catalyst volume (or weight) is increased. The effect of the space velocity on CO and H_2 yield (constant yields or increasing selectivity) is another proof that CO and H_2 are primary reaction products over 12% Ru/Al_2O_3 catalysts [24].

4.2. Evolution of $RuO_2 \Leftrightarrow Ru$ equilibrium under reaction conditions

The results of the catalytic, XRD, TPO, and TPR investigations suggest that the formation of methane oxidation products is governed by the $RuO_2 \Leftrightarrow$ Ru equilibrium. The ignition temperature is very sensitive to the oxidation state of the metal prior to ignition. For example it was observed that the deactivation of Rh and Ir is most likely the result of the formation of a relatively stable surface oxide under fuel-lean conditions [19]. The partial oxidation of methane starts at the moment when most of bulk RuO_2 is reduced under reaction conditions to Ru metal by the O_2/CH_4 mixture. If this assumption is correct, then the nature of oxidizing as well as reducing agents should have an influence on the $RuO_2 \Leftrightarrow$ Ru equilibrium. A stronger oxidizing agent would increase the rate of metal reoxidation in comparison with that of oxide reduction by CH_4. Fig. 9 presents the influence of the oxidizing agent on the ignition temperature of POM reactions using as catalyst 12% Ru/Al_2O_3. For both oxidants used (O_2 and NO) the C/O ratio in the reactant mixture was close to one. Fig. 9 shows that the ignition temperature was higher by 100 °C when NO (550 °C $< T_{\text{ignition}} <$ 600 °C) was used as an oxidizing agent instead of O_2 (450 °C $< T_{\text{ignition}} <$ 500 °C). The distribution of the reaction products (not shown here) is similar for both oxidants used, suggesting a similar reaction mechanism. The temperature gap observed between the light-off temperatures of NO/CH_4 and O_2/CH_4 reactions can be explained as follows. The first step in metal oxidation is the dissociation of O–O or N–O bonds. The O–O bond energy of 498 kJ mol^{-1} is significantly higher than that of N–O (200.6 kJ mol^{-1}) [25]. The decomposition of NO at low temperature leaves strongly adsorbed oxygen on the surface, which blocks the metal sites for methane activation [26,27]. The surface O will further react rapidly with Ru metal to form bulk RuO_2. On the other hand, O–O dissociation will take place at higher temperatures as compared with NO, given the higher bond activation energy. Therefore, NO is a stronger oxidizer than O_2 in the low temperature domain. The increase in reaction temperature will trigger the reduction of RuO_2 by methane. The relative rate of RuO_2 reduction can be expressed as the difference between the rate of oxide reduction and the rate of reoxidation. It is rational to consider that, for equivalent CH_4 in the reaction mixture, the *relative* reduction rate of RuO_2 will be related to the nature of the oxidizing agent. Taking into account the bond energies, it is clear that the formation of RuO_2 is faster in NO than in O_2. In fact, the reaction inflammation depends on the ability of an oxidant/CH_4 mixture to shift the $RuO_2 \Leftrightarrow$ Ru equilibrium to the formation of Ru metal. It can be said that the state of ruthenium is a mirror of reaction conditions.

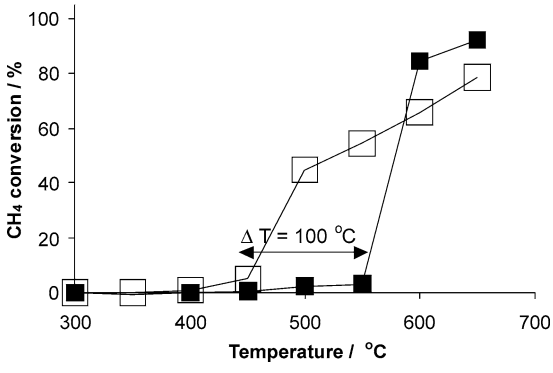

Fig. 9. The comparative methane conversion over 12% Ru/Al_2O_3 catalysts using as oxidant O_2 (□) and NO (■). The C/O ratio for both oxidants used was close to the stoichiometric one (mixture I, 10.5% CH_4 and 5.8% O_2 in N_2; mixture II, 10.5% CH_4 and 13% NO in Ar).

The $RuO_2 \Leftrightarrow$ Ru equilibrium under reaction conditions is also related to the particle size. It is likely that above the ignition point the larger Ru particles will preserve better their metal state as compared with well-dispersed ones [28]. Thus, it is expected to have enhanced catalytic activity for CH_4 conversion and selectivity to CO and H_2 over large Ru nanoparticles. The experimentally observed reaction yield to CO and H_2 over large Ru nanoparticles (initial size 5.8 nm, used catalyst ≈ 14 nm) at 650 °C was 72.1 and 67.6%, respectively (see Fig. 3). The yield to syn gas was found to be significantly lower for the classically prepared Ru-based catalyst. For example, the reported yields to CO and H_2 at 800 °C over TiO_2-supported Ru nanoparticles of around 3 nm were only 20.8 and 33.1%, respectively [29]. Moreover, the catalytic performance of our catalyst is comparable with that of Ni-based catalysts (syn gas yield ≈ 73%) operating in the 750–1000 °C temperature range [13,30].

The XRD results depicted in Fig. 6 support also the idea of progressive reduction of RuO_2 to Ru metal with increasing in the reaction temperature. For O_2–CH_4 reactions, the XRD reflection of RuO_2 for the catalyst working at 450 °C (kinetic region) can be well observed at $2\theta = 28$ and 54° (Fig. 6A, spectrum c). On the other hand, the active catalysts at 550 and 650 °C show only diffuse, hardly distinguishable RuO_2 XRD peaks (Fig. 6A, spectra d and e). In the case of NO–CH_4 reactions, the formation of an abundant RuO_2 phase was detected at 450 and 550 °C whereas the XRD reflections characteristic for Ru metal were absent (Fig. 6B, spectra f and g). However, at 650 °C most of the RuO_2 was converted to Ru metal because the XRD peaks of RuO_2 could not observed (Fig. 6B, spectrum h). The slower reduction of RuO_2 by NO–CH_4 mixtures ($\Delta T \approx 100$ °C) is reflected also by a catalytic behavior. The light-off temperature over Ru/A_2O_3 catalyst is higher at 100 °C for NO–CH_4 reactions as compared to O_2–CH_4 reactions (Fig. 9).

The TPR results, in line with the XRD data, show clearly a progressive shift of $RuO_2 \Leftrightarrow$ Ru equilibrium to Ru metal with increasing reaction temperature (Fig. 7). Once the reac-

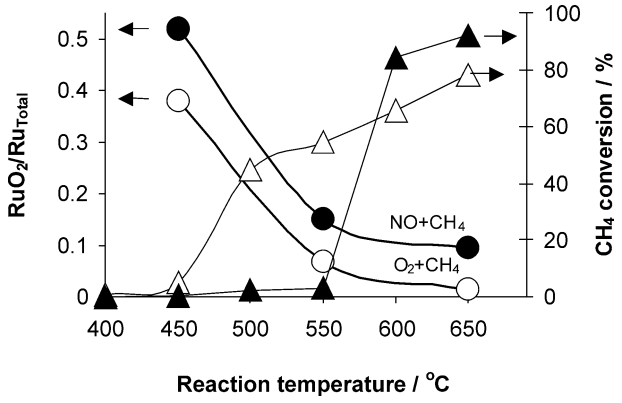

Fig. 10. Relationship between the amount of RuO_2 (expressed as fraction of total Ru) formed during partial oxidation of methane with O_2 (○) and NO (●) over 12% Ru/Al_2O_3 catalysts and reaction temperature. Additionally, the conversion of CH_4 with O_2 (△) and NO (▲) vs temperature is also represented. Reaction mixtures were 10.6% CH_4 and 5.9% O_2 (balance N_2) and 10.5% CH_4 and 13% NO (balance Ar).

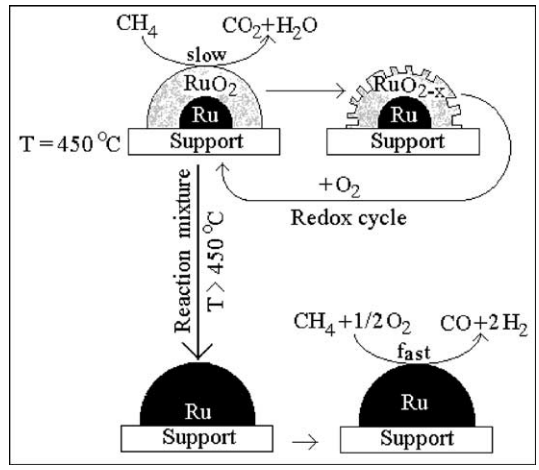

Fig. 11. Simplified model describing the mechanism of O_2/CH_4 reaction over alumina-supported Ru nanoparticles.

tion becomes ignited, the decrease in RuO_2 amount is sharp, especially in O_2–CH_4 mixtures.

The chemical state of the active catalyst exposed to O_2–CH_4 and NO–CH_4 mixtures at 450, 550, and 650 °C was estimated by quantifying the amount of consumed H_2 during the TPR runs. The evolution of RuO_2/Ru ratio with reaction temperature is illustrated in Fig. 10. In the case of the O_2–CH_4 system, the experimentally determined values for RuO_2/Ru_{Total} fractions were 0.37 at 450 °C, 0.07 at 550 °C, and 0.01 at 650 °C (Fig. 10, ○). The abrupt reduction of RuO_2 under reaction conditions, along with the change in products distribution, explains well the switch of the mechanism observed in the 450–500 °C temperature range. The RuO_2/Ru_{Total} fraction for the catalyst used for NO–CH_4 reaction showed also a decreasing trend reaction temperature. Under the same conditions, larger amounts of RuO_2 always were formed when NO was used as oxidizing agent instead of O_2. The experimentally determined RuO_2/Ru_{Total} fractions for the NO–CH_4 system at 450, 550 and 650 °C were 0.51, 0.15, and 0.10, respectively (see Fig. 10, ●). From Fig. 10 it can also be observed that the sudden increase in CH_4 conversion is taking place for low RuO_2/Ru_{Total} ratios (i.e., ≈ 0.10). In other words, the changes of the reaction rate and mechanism are closely related to the state of the alumina-supported Ru.

Many of the contradictory reports concerning the formation of primary reaction products can be explained in light of our experimental data. For example, Weng et al. [6] observed (by FTIR) that at 600 °C the formation of CO_2 proceeds much earlier than that of CO. Their conclusion pointed out that CO_2 is the primary reaction product. In fact, the time lag between CO and CO_2 (induction period) formation can be explained by the progressive reduction of RuO_2 to Ru metal phase in the reaction mixture. Our experimental data show clearly that CO (and H_2) can be formed only on Ru metal. Thus, it becomes clear that the formation of CO and H_2 is related more to the chemical state and morphology (size) of ruthenium particles than to the secondary CO_2/CH_4 and H_2O/CH_4 shift reactions. The induction period (faster formation of CO_2 as compared with H_2 and CO) observed also by isotope tracing experiments [7] can be interpreted in the same manner. The assumption that CO and H_2 are the primary reaction products is sustained by other facts, too. Hickman and Schmidt [23] reported that for short contact time (< 0.01 s), the primary reaction products are H_2 and CO because the secondary reactions, such as steam reforming and water–gas shift reactions, are slow processes. Thermodynamic calculations for POM reactions differ significantly from our experimental data [1]. For example, at 600 °C the theoretically predicted data for H_2/CO and CO_2/CO ratios are 2.5 and 1, respectively, whereas our experimental values for the same ratios are 1.8 and 4.8. The deviation of our data from the thermodynamic equilibrium values is another proof that the product distribution is insignificantly affected by equilibrium reactions.

In summary a simplified mechanism of O_2/CH_4 reaction over alumina-supported Ru catalyst is proposed in Fig. 11. For temperatures $\leqslant 450$ °C, CH_4 is selectively oxidized to CO_2 and H_2O over bulk RuO_2 probably by a Mars van Krevelen redox-type mechanism [16]. The activity of RuO_2 for methane oxidation is low. In the first stage some of the bulk RuO_2 is reduced by CH_4 forming substoichiometric oxide (RuO_{2-x}). This process is viewed as a creation of surface oxygen vacancies (surface defects) [16]. In parallel with RuO_2 reduction, CH_4 is oxidized to CO_2 and H_2O. Since the rate of methane oxidation is low (low sticking coefficient), the oxide layer is not completely depleted to metal because the reoxidation (refilling of oxygen vacancies) with gas-phase O_2 is a faster process at 450 °C. The increase in reaction temperature leads to the acceleration of RuO_2 reduction until the Ru metal becomes the dominant phase. The enrichment of the catalyst in Ru metal during POM reaction was suggested also by XPS investigations [4]. Other POM catalysts, such as Ni/Yb_2O_3, are also active/selective only in their reduced form [31]. Over Ru metal, the mechanism

and the reaction rate change suddenly, and the reaction becomes ignited. Surface reactions which produce H_2 and CO occur in an oxygen-depleted environment, and the major surface species are probably adsorbed C or CH_x and H [23]. It is known that the adsorbed CH_4 dissociates on the surface of Ru metal in CH_x species (CH, C–CH_2, C–CH_3, and graphitic carbon) and H [32]. The CH_x species form different types of carbon deposits on the Ru surface, depending on the reaction conditions (i.e., carbidic, amorphous, and graphitic) [33]. The surface hydrogen-poor carbonaceous species react with oxygen to produce CO, which desorbs before being further oxidized to CO_2.

5. Conclusions

The O_2/CH_4 reaction mechanism was found to be related to the chemical state and size of the alumina-supported Ru nanoparticles. In the kinetic region (350–450 °C) ruthenium nanoparticles are extensively oxidized by the reaction mixture ($CH_4/O_2 = 1.8$) to RuO_2. Over RuO_2, CH_4 is converted slowly and selectively to CO_2 and H_2O. The further increase in reaction temperature ($T > 450$ °C), favoring the reduction of RuO_2 to Ru metal by the reaction mixture, triggers the reaction ignition. Large amounts of CO and H_2 are generated simultaneously as a result of the change in reaction mechanism. Above the ignition temperature, the reaction rate and product distribution are significantly affected by mass transport effects. The ignition temperature is related to the oxidation–reduction kinetics of the supported Ru nanoparticles. Thus, the nature of the oxidant, the morphology (size) of the Ru nanoparticles, and the composition of the reaction mixture are essential factors in determining the mechanism of the partial oxidation of methane.

The large Ru nanoparticles prove to be more effective in enhancing the reaction yield to CO and H_2 because, above the ignition point, they preserve better the metal character under reaction conditions, as compared with the small Ru particles of the conventionally prepared catalysts.

Acknowledgment

The authors are grateful to Dr. C. Contescu for his valuable insight in the present work.

References

[1] S.C. Tsang, J.B. Claridge, M.L.H. Green, Catal. Today 23 (1995) 3.
[2] J.N. Armor, Appl. Catal. A 176 (1999) 159.
[3] I. Balint, A. Miyazaki, K. Aika, J. Catal. 207 (2002) 66.
[4] A.T. Ashcroft, A.K. Cheetham, J.S. Foord, M.L.H. Green, C.P. Grey, A.J. Murrell, P.D.F. Vernon, Nature 344 (1990) 319.
[5] C. Elmasides, X.E. Verykios, J. Catal. 203 (2001) 477.
[6] W.Z. Weng, M.S. Chen, Q.G. Yan, T.H. Wu, Z.S. Chao, Y.Y. Liao, H.L. Wan, Catal. Today 63 (2000) 317.
[7] A. Guerrero-Ruiz, P. Ferreira-Aparicio, M.B. Bachiller-Baeza, I. Rodriguez-Ramos, Catal. Today 46 (1998) 99.
[8] C. Elmasides, D.I. Kondarides, W. Grünert, X.E. Verykios, J. Phys. Chem. B 103 (1999) 5227.
[9] P. Ferreira-Aparicio, I. Rodriguez-Ramos, A. Guerrero-Ruiz, Appl. Catal. A 148 (1997) 343.
[10] A. Miyazaki, I. Balint, K. Aika, Y. Nakano, J. Catal. 204 (2001) 364.
[11] D.A. Frank-Kamenetskii, Diffusion and Heat Transfer in Chemical Kinetics, Plenum, New York, 1969, pp. 460–465.
[12] P. Aghalayam, Y.K. Park, N. Fernandes, V. Papavassiliou, A.B. Mhadeshwar, D.G. Vlachos, J. Catal. 213 (2003) 23.
[13] M.A. Peña, J.P. Gómez, J.L.G. Fierro, Appl. Catal. A 144 (1996) 7.
[14] J. Zhu, D. Zhang, K.D. King, Fuel 80 (2001) 899.
[15] P. Gallezot, in: J.R. Anderson, M. Boudart (Eds.), Catalysis; Science and Technology, Vol. 5, Springer, Berlin, 1984, p. 226, Chapt. 4.
[16] H. Madhavaram, H. Idriss, S. Wendt, Y.D. Kim, M. Knapp, H. Over, J. Aßmann, E. Löffler, M. Muhler, J. Catal. 202 (2001) 296.
[17] P. Betancourt, A. Rives, R. Hubaut, C.E. Scott, J. Goldwasser, Appl. Catal. A 170 (1998) 307.
[18] O. Deutschmann, F. Behrendt, J. Warnatz, Catal. Today 46 (1998) 155.
[19] G. Veser, M. Ziauddin, L.D. Schmidt, Catal. Today 47 (1999) 219.
[20] Y.-F. Chang, H. Heinemann, Catal. Lett. 21 (1993) 215.
[21] M.F.M. Zwinkels, G.M.E. Heginuz, B.H. Gregertsen, K. Sjöström, S.G. Järås, Appl. Catal. A 148 (1997) 325.
[22] A.F. Ahlström-Silversand, C.U.I. Odenbrand, Appl. Catal. A 153 (1997) 157.
[23] D.A. Hickman, L.D. Schmidt, J. Catal. 138 (1992) 267.
[24] K. Nakagawa, N. Ikenaga, T. Suzuki, T. Kobayashi, M. Haruta, Appl. Catal. A 169 (1998) 281.
[25] E.J.A. Dean, Lange's Handbook of Chemistry, 11th ed., McGraw-Hill, New York, 1973, pp. 3–126.
[26] A.V. Walker, M. Gruyters, D.A. King, Surf. Chem. 384 (1997) L791.
[27] P.-A. Bui, D.G. Vlachos, P.R. Westmoreland, Surf. Sci. 385 (1997) L1029.
[28] M. Boudart, J. Mol. Catal. 30 (1985) 27.
[29] C. Elmasides, T. Ioanides, X.E. Verykios, AIChE 46 (2000) 1260.
[30] H.-S. Roh, K.-W. Jun, W.-S. Dong, S.-E. Park, Y.-I. Joe, Chem. Lett. (2001) 666.
[31] V.R. Choudhary, A.M. Rajput, V.H. Rane, J. Phys. Chem. 96 (1992) 8686.
[32] T.V. Choudhary, D.W. Goodman, J. Mol. Catal. A 163 (2000) 9.
[33] M.C. Bradford, J. Catal. 189 (2000) 238.